

Growth mode, magnetic and magneto-optical properties of pulsed-laser-deposited Au/Co/Au(111) trilayers

C. Clavero,^{1,*} A. Cebollada,¹ G. Armelles,¹ and O. Fruchart²

¹*Instituto de Microelectrónica de Madrid-IMM (CNM-CSIC),
Isaac Newton 8 (PTM), 28760 Tres Cantos, Madrid, Spain*

²*Institut Néel (CNRS & UJF), BP166, F-38042 Grenoble, Cedex 9, France*
(Dated: December 4, 2018)

The growth mode, magnetic and magneto-optical properties of epitaxial Au/Co/Au(111) ultrathin trilayers grown by pulsed-laser deposition (PLD) under ultra-high vacuum are presented. Sapphire wafers buffered with a single-crystalline Mo(110) bilayer were used as substrates. Owing to PLD-induced interfacial intermixing at the lower Co/Au(111) interface, a layer-by-layer growth mode is promoted. Surprisingly, despite this intermixing, ferromagnetic behavior is found at room temperature for coverings starting at 1 atomic layer (AL). The films display perpendicular magnetization with anisotropy constants reduced by 50% compared to TD-grown or electrodeposited films, and with a coercivity more than one order of magnitude lower ($\lesssim 5$ mT). The magneto-optical (MO) response in the low Co thickness range is dominated by Au/Co interface contributions. For thicknesses starting at 3 AL Co, the MO response has a linear dependence with the Co thickness, indicative of a continuous-film-like MO behavior.

PACS numbers:

I. INTRODUCTION

Owing to its ability to essentially preserve the stoichiometry of targets during evaporation, Pulsed-Laser Deposition (PLD) is often used for the growth of materials with a complex composition, particularly oxides such as high- T_c superconductors, ferroelectrics and manganites¹. When performed under ultra-high vacuum conditions PLD is also suitable for the epitaxy of metals², although it is seldom used for that purpose. There are two main differences between PLD and Thermal Deposition (TD) concerning the epitaxy of metals. The first difference is the possibility to force layer-by-layer growth in some cases³, which is a positive aspect. This fact arises from the several orders of magnitude higher instantaneous deposition rate during the laser pulse duration and from the increased kinetic energy of the ejected species (up to several eV) as compared with TD⁴. The second aspect is to potentially induce some intermixing at interfaces⁵, which may be a drawback to reach certain physical properties depending on the smoothness of interfaces. Evidence of an increased tendency of intermixing at interfaces in structures grown by PLD versus TD has been given previously by X-ray diffraction⁵, and it is generally thought to result from the energy carried by the atoms or ions evaporated from the target and heated upon further interaction with the laser in the plume⁴. Here we report on the growth by PLD and the resulting magnetic and magneto-optical (MO) properties of epitaxial Au/Co/Au trilayers, motivated by the observed perpendicular magnetic anisotropy in TD grown⁶ or electrodeposition(ED)⁷ Co/Au(111) films capped with various materials.

In this work the Au surface used as substrate is a thin (111) film deposited on a buffer layer of refractory metal [Mo(110)] epitaxially grown on Sapphire (11 $\bar{2}$ 0). For this

particular set and order of elements (*i.e.*, Co deposited on Au) we evidence by scanning tunneling microscopy some intermixing at the Au/Co interface, inducing a layer-by-layer growth for Co as compared to a two-atomic-layer-high-island growth for TD. Interestingly, despite the intermixing ferromagnetic behavior is found at room temperature for coverings starting at 1 atomic layer (AL). An easy axis of magnetization is found perpendicular to the plane for Co coverings between 1 and 5 AL, with magnetic anisotropy constants similar to their TD or ED counterparts, however with a much lower coercivity. The spectroscopic magneto-optical activity of the films has also been measured and modeled.

II. EXPERIMENTAL

The samples were grown by pulsed laser deposition (PLD) under ultrahigh vacuum (UHV) inside a three-chamber setup⁸. The first chamber is devoted to preparation and analysis. It is equipped with a heater for sample degassing up to 800 °C, a sputtering gun and an Auger electron analyzer. The base pressure is 2×10^{-10} Torr. The second chamber is the deposition chamber. It is equipped with a 10 keV reflection high-energy electron diffraction (RHEED) setup, a quartz microbalance, and a sample heating similar to that of the first chamber. The base pressure is $2 - 3 \times 10^{-11}$ Torr and in the 10^{-10} Torr range during laser deposition. A third chamber is dedicated to Scanning Tunneling Microscopy (STM) with a room temperature (RT) Omicron-1 setup (base pressure 5×10^{-11} Torr). A Nd-YAG laser with a 10 ns pulse duration and a 10 Hz frequency was used. The targets are first mechanically polished *ex situ* and then surface-cleaned *in situ* through laser ablation until no gas contaminant is found on the target, as controlled by

Auger spectroscopy. The targets are cleaned at the same fluence as that used during the growth (about 1 J/cm^2). This sequence is chosen for each element just above the evaporation threshold, so as both to avoid the formation of droplets⁹ and to minimize the energy carried by evaporated individual atoms or ions⁴. Under these conditions the typical growth rate on the sample is 1 \AA/s . More details can be found in Ref.⁸.

Hysteresis loops were carried out by means of a Superconducting Quantum Interference Device (SQUID) magnetometer at low and RT. The magneto-optical (MO) polar response of the samples was studied experimentally in the spectral range from 1.4 to 4.3 eV, using a spectrometer described elsewhere¹⁰.

III. AU(111) SURFACE PREPARATION

We used commercial sapphire($11\bar{2}0$) wafers with a miscut angle smaller than 0.1° . A 10 nm-thick buffer layer of Mo(110) was first deposited following an optimized procedure^{8,11}. Its surface is single-crystalline and displays $\approx 200 \text{ nm}$ -wide terraces separated by monoatomic steps. The steps separation and orientation are determined by the miscut of Sapphire, which is uniform on a two-inch wafer, however varies from one wafer to another. This residual miscut, on the average smaller than that typically found on metal single-crystals, does not influence the growth mode and thus presumably neither the magnetic properties.

Next a 5 nm-thick Au film was deposited at RT on top of the Mo buffer layer. The Au surface was then sputtered with 1 kV Ar^+ ions to remove a few AL, then annealed at 550°C during 30 minutes. The resulting Au surface was studied by STM. It is atomically-flat with the usual $22 \times \sqrt{3}$ reconstruction of Au^{12,13,14}. However the presence of micro-grain-boundaries and dislocation loops prevent the occurrence of a perfect long range herringbone superstructure as for Au single crystals (FIG. 1), its appearance being limited to restricted areas as shown in the zoom to FIG. 1.

IV. CO GROWTH ON AU(111)

FIG. 2 shows STM pictures of various amounts of Co deposited at RT on the Au surfaces described above. In the sub-atomic-layer range Co growth proceeds through the more-or-less random nucleation of 1 AL-high islands. The distribution of island lateral size is quickly bimodal (FIG. 2 b-c) owing to the combination of homogeneous nucleation by adatom aggregation and heterogeneous nucleation on the Au(111) defects^{15,16}. The growth in this sub-atomic-layer range dramatically differs from the case of TD, for which the islands are 2 AL-high and nucleate almost solely at the elbows of the Au herringbone reconstruction¹⁷, with a random 0.02 nm corrugation on the top of the islands owing to the large mismatch be-

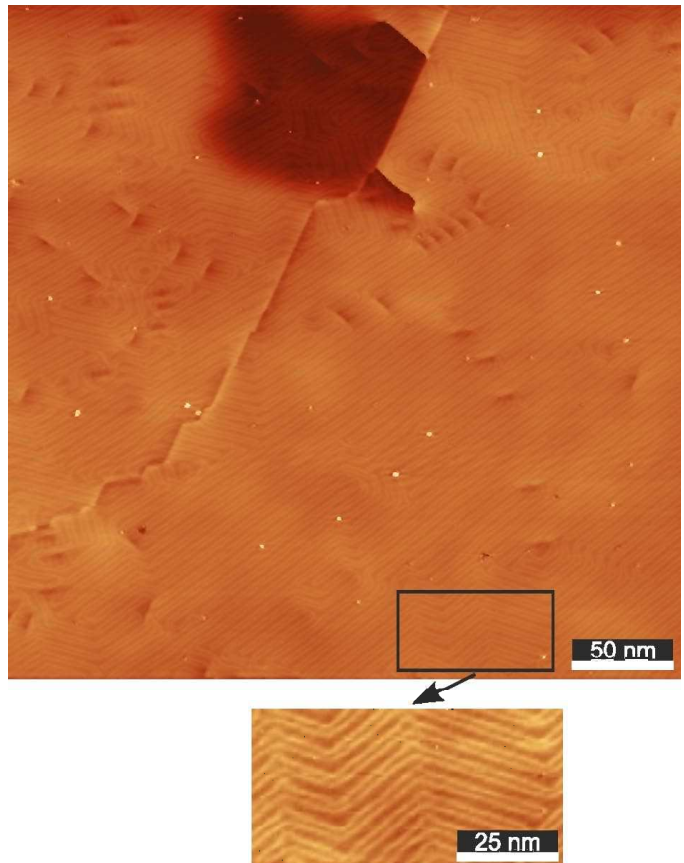


FIG. 1: (Color online) $375 \times 375 \text{ nm}$ STM image of Au(111) grown on Mo(110) (sample voltage 1 V, current 0.25 nA). The gray scale has been adjusted between zero and the maximum height $Z_{max}=1.5 \text{ \AA}$. A zoom of a selected area is shown in the lower part, displaying the Au(111) herringbone reconstruction with $Z_{max}=0.54 \text{ \AA}$.

tween Co and Au^{18,19}. Here, stripe-like areas of two different heights are observed on the top of the 1 AL-high Co islands, as the zoom of a selected area in FIG. 2 (b) shows (note that the vertical scale in this $25 \times 25 \text{ nm}$ area has been optimized to better display the top part of the islands). This feature points to some degree of intermixing between Co and Au as previously observed in PLD deposited systems⁵. As above mentioned, the interfacial intermixing in PLD is a result of the energy carried by the atoms or ions evaporated from the target and heated upon further interaction with the laser in the plume^{4,5}. Although we set the laser fluence just above the evaporation threshold, tails in the energy distribution or hot spots in the laser beam may create a small fraction of atoms or ions carrying a few eV or more. Notice that interfacial intermixing is not a systematic feature of PLD, as we did not observe such inhomogeneities in other systems, e.g. Fe²⁰ or Co deposited on W or Mo(110). The higher bonding energy of the latter with respect to Au may prevent the intermixing. The growth mode of further Co layers proceeds close to a layer-by-layer fashion, with a morphology and inter-island distances at 4 AL

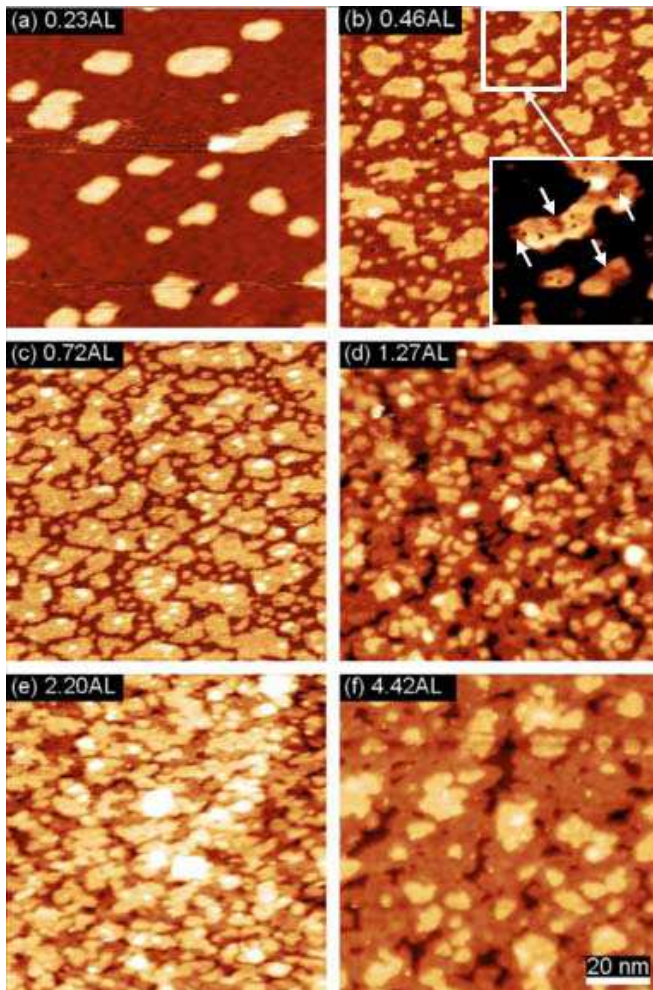


FIG. 2: (Color online) 100x100 nm STM images of PLD-grown Co/Au(111) films at various coverages, expressed in atomic layers (AL). After random nucleation at the first stages of growth (a), a bimodal distribution of islands with stripe-like corrugation is observed for submonoatomic coverings (b)-(c). The 25x25 nm zoom in (b) shows a stripe-like corrugation on the islands (note that the vertical scale was optimized in this case to better show the top of the islands. White arrows point at some of the lower areas on the islands). The growth of further layers proceeds close to a layer-by-layer fashion (d)-(f). The gray scale has been properly adjusted in each case between zero and the maximum height Z_{\max} , with $Z_{\max} = 4.2, 5.3, 5.3, 5.5, 5.4$ and 6.1 \AA for images (a), (b), (c), (d), (e) and (f) respectively. Z_{\max} is 1.4 \AA for the inset to (b).

of approximately 20 nm, very similar to those obtained with TD²¹. Thus the topography of PLD-grown films a few AL thick is similar to their TD-grown counterparts, except for some intermixing at the bottom interface.

V. MAGNETIC ANISOTROPY AND HYSTERESIS

Magnetization characterization was performed on samples similar to those presented above, however immediately capped with a 2 nm thick Au layer *in situ* for protection against contamination (*i.e.*, with no STM investigation). The magnetization reversal of 1, 3 and 5 AL-thick Co samples was studied by means of SQUID magnetometry, under successively in-plane and perpendicular magnetic fields, at low (FIG. 3) and RT (FIG. 4). Surprisingly, ferromagnetic behavior is found in all the PLD films at RT for Co coverings starting at 1 AL grown. This is a striking result since TD films of nominal thickness 1.5 AL and below are not ferromagnetic at RT⁶. The lower ferromagnetic critical thickness found in our PLD films stems from the different growth mode observed between both techniques. As above mentioned, for TD films Co nucleates in the form of isolated 2 AL-thick islands in relation to the herringbone reconstruction of Au(111)^{12,14}, forming crystallites of ultimately 6-10 nm in diameter²², which remain superparamagnetic until percolation occurs around 1.6 ML²³. On the other hand, in our case PLD leads to 1 AL-high Co islands at the early stages of growth, with larger lateral extends as compared to TD films (irregularly shaped islands up to 25 nm long are found at coverings around 0.72 AL as shown in FIG. 2 (c)), with percolation starting at submonoatomic coverings, and thus favoring the observed ferromagnetic behavior. The accuracy of saturation magnetization M_s measurements using SQUID on magnetic thin films is subject to several factors, including error on the estimation of the volume of the magnetic films and background diamagnetic signals that must be subtracted. After correction of the measured data, saturation magnetization values close to the bulk value ($M_s = 1.446 \times 10^6 \text{ A/m}$) were found for the 3 and 5 AL-thick Co films, whereas a reduction around 30% was found for the 1 AL-thick film owing to the above mentioned interdiffusion of Co and Au, being this effect specially important in the low thickness regime.

Interestingly, the 100% remanence along the direction perpendicular to the plane and the almost closed loops in-the-plane demonstrate a full perpendicular anisotropy for all the coverings and measurement temperatures, as shown in FIG. 3 and FIG. 4. We analyze the magnetic anisotropy energy (MAE) at low temperature to access the values in the fundamental state. The density of MAE was computed from the hysteresis loops along the perpendicular direction as $K = \mu_0 \int_0^{M_s} H dM$. The resulting values are summarized in TABLE I. The MAE increases at low thickness, consistently with the picture of a dominant contribution of interface and/or magneto-elastic terms^{24,25}.

Concerning the easy axis of magnetization, the coercivity depends only weakly on the thickness. It decreases from around 30-40 mT at low temperature to typically 3-5 mT at RT. This sharp decrease with temperature is

TABLE I: Directly-measured total density of magnetic anisotropy energy at 10 K (in MJ/m³) for Au/Co/Au films fabricated by PLD.

1 AL	3 AL	5 AL
0.91	0.65	0.32

common for ultrathin films because the activation volumes involved in nucleation or activation processes underlying magnetization reversal²⁶ are small as they scale with the thickness of the film^{27,28}. Thermal activation is therefore much enhanced compared to bulk materials. Previously Au/Co/Au films had been extensively prepared using TD⁶ and more recently with ED⁷. Both exhibit perpendicular anisotropy up to about ten AL of Co. Their total MAE has been measured mostly for films 5 AL and thicker. For 5 AL figures in the range 0.7-0.8 MJ/m³ have been given^{6,7}. This is roughly double the MAE of 5 AL-PLD-grown films (TABLE I). This reduced value for our films may result from the intermixing at their lower interface. Comparison at lower thicknesses based on extrapolation using published values of volume and surface energies may be hazardous and thus is not discussed here, although a similar reduction would be expected. The case of coercivity is more striking. The coercivity at RT of 3-5 AL TD or ED films are typically in the range 35-80 mT depending on the preparation conditions^{27,29,30}. This is more than one order of magnitude higher than for our PLD films, an effect which obviously cannot be ascribed solely to the 50 % decreased MAE. Instead we ascribe this to the difference of growth modes, as it was done for the early onset of ferromagnetic behavior. In TD and ED the growth initially proceeds by the formation of 2 AL-high islands. This induces a significant roughness that may be responsible for the high coercivity, whereas the initial AL-growth with PLD yields smoother films, topographically and obviously magnetically. This allows the occurrence of ferromagnetism however still associated with a high coercivity as the domain wall propagation is hindered between islands. Already at 1 AL PLD films combine both ferromagnetism and a low coercivity owing to the initial growth mode in 1 AL-high islands.

Let us summarize the discussion of the relationship between the growth-modes-related microstructure and magnetic properties. Owing to the intermixing-induced initial growth mode as 1 AL-islands, PLD films compared to TD or ED films have ferromagnetic ordering already at 1 AL, a MAE reduced by $\approx 50\%$ and a coercivity more than one order of magnitude lower.

VI. MAGNETO-OPTICAL (MO) ACTIVITY

The magneto-optical (MO) properties of Au/Co/Au trilayers and Au/Co multilayers grown by TD as a function of the Co thickness have been extensively

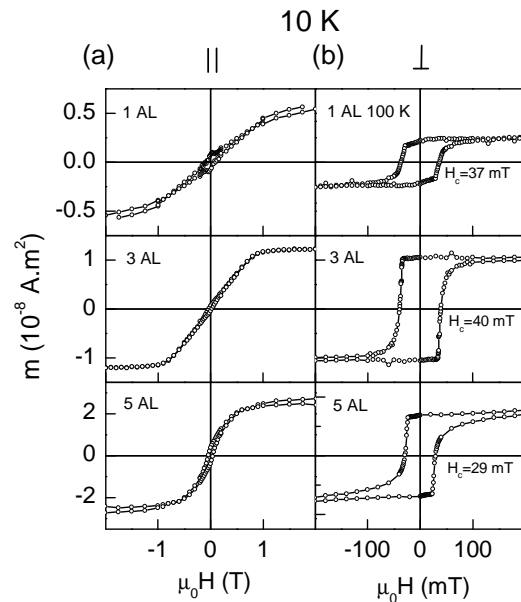


FIG. 3: SQUID hysteresis loops performed at low temperature for Co films of 1, 3 and 5 AL, both in-plane (left column) and perpendicular to the plane (right column). All loops have been measured at 10 K except the perpendicular loop of the 1 AL-thick film, which was measured at 100 K.

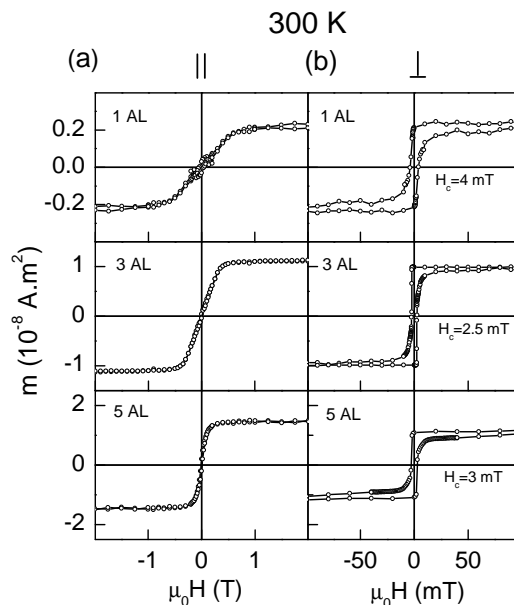


FIG. 4: SQUID hysteresis loops performed at RT for Co films of 1, 3 and 5 AL, both in-plane (left column) and perpendicular to the plane (right column).

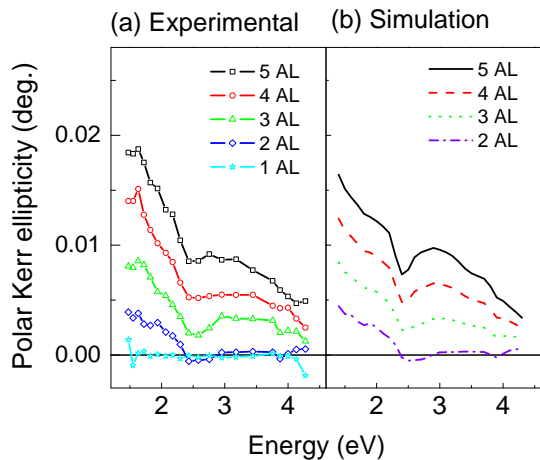


FIG. 5: (Color online) (a) Experimental and (b) simulated polar Kerr ellipticity spectra for the systems with Co films ranging from 1 and 5 AL.

studied^{31,32,33,34,35,36}. Višňovský et al.^{31,32,33} showed that the MO response of these systems in the thin film limit is given by the sum of one independent plus one linearly dependent term on the Co film thickness. They ascribed the independent term to different Au/Co interface effects, such as Au-Co mismatch driven stress, lattice defects, Au-Co electronic orbital hybridization and intermixing at the interface³¹. More recently, Hamrle et al.³⁴ studied specifically the contribution of Co/Au interfaces to the MO response of Au/Co/Au trilayers, and concluded that the most important part of the interface contribution arises from intrinsic properties of the interface itself, i.e., from the Au-Co electronic hybridization. Nevertheless, no studies about the MO response of similar PLD grown structures have been reported so far.

Here, the MO characterization was performed on the samples presented in Section V, with graded Co thicknesses from 1 to 5 AL. Polar Kerr ellipticity spectra were measured in the spectral range from 1.4 to 4.3 eV. In this configuration, normal incident light is used, being the polarization change of the reflected light (rotation and ellipticity) measured with magnetic field applied perpendicular to the surface. As shown in FIG. 5 (a), almost zero ellipticity is obtained for 1 AL, whereas a progressive increase is observed as the Co thickness increases over the entire spectral range, in accordance with previous reports on TD-grown systems^{33,34}. In addition, the characteristic peak arising from the Au plasma edge is found in all the cases around 2.5 eV^{31,32,33,35}.

In order to model the evolution and shape of the ellipticity spectra, simulations were performed using the transfer matrix formalism³⁷. As shown in FIG. 5 (a), a strong effect on the ellipticity spectra due to the Au/Co interfaces is observed for the trilayers with 1 and 2 AL thick Co films, exhibiting values smaller than expected for such Co thickness considering bulk MO constants³⁸, in agreement with previous reports³¹. In principal, the

MO response of both Au/Co interfaces in the trilayers can be described by the measured MO response of the trilayer with a 2 AL thick Co film, since, as above mentioned, the MO response can be ascribed to short range Au-Co hybridization effects involving only the atomic layers closer to the interface, and in this case also some short range degree of intermixing as observed with STM. Thus, under the ultra thin film approach³³, the ellipticity of the trilayers with 3, 4 and 5 AL layers thick Co films can be simulated by adding the ellipticity of 1, 2 and 3 Co thick continuous films respectively, addressing the inner part of the Co film unaffected by the interface, and the ellipticity of the trilayer with a 2 AL thick Co film, addressing the interface effects. The optical constants for Mo, Co and Au were obtained from Ref.³⁹ whereas bulk MO constants for Co were used³⁸. In fact, as shown in FIG. 5 (b), simulations yield a good agreement with the measured spectra in intensity and shape for the simulated 3, 4 and 5 AL Co coverages. These results confirm that the MO response in the low Co thickness range is dominated by Au/Co interface effects, the ellipticity showing a linear response with the Co thickness for thicknesses starting at 3 AL Co, indicative of a continuous-film-like MO behavior in accordance with TD grown systems^{31,33,34,35}.

VII. CONCLUSION

We fabricated epitaxial Co ultrathin films by pulsed-laser deposition on sapphire wafers buffered with a Au/Mo layer. Unlike TD-grown films which require 1.6 AL to become ferromagnetic, ferromagnetic behavior is found at room temperature for coverings starting at 1 AL. The films display perpendicular magnetization with magnetic anisotropy energy reduced by $\approx 50\%$ compared to TD-grown or electrodeposited films, and an unprecedented low coercivity of ≈ 5 mT. We ascribed these differences to some degree of intermixing at the lower interface upon PLD. This reduces surface anisotropy, however promotes a layer-by-layer growth and thus yields a topographically and magnetically smoother film. The magneto-optical response in the low Co thickness range is dominated by Au/Co interface contributions. For thicknesses starting at 3 AL Co, the MO response has a linear dependence with the Co thickness, indicative of a continuous-film-like MO behavior.

VIII. ACKNOWLEDGMENTS

We acknowledge financial support from FP6 EU-NSF program (STRP 016447 MagDot), French National Research Agency (ANR-05-NANO-073 Vernanomag), “FUNCOAT” CONSOLIDER INGENIO 2010 CSD2008-00023, “NANOMAGMA” EU NMP-FP7-214107, “MAGPLAS” MAT2008-06765-C02-01/NAN, MAT2005-05524-C02-01 and “NANOMAGNET” CM S-

0505/MAT/0194. CC acknowledges the Ministerio de Educación y Ciencia through the FPI program and R. A. Lukaszew for financial support. We are grateful to J.

Ferré (LPS-Orsay) for both preliminary measurements and a critical reading of the manuscript.

-
- * Current address: Department of Applied Science, College of William & Mary, Williamsburg, Virginia 23187, USA. cclavero@wm.edu
- ¹ J. S. Horwitz, D. B. Chrisey, R. M. Stroud, A. C. Carter, J. Kim, W. Chang, J. M. Pond, S. W. Kirchoefer, M. S. Osofsky, and D. Koller, *Appl. Surf. Science* **127-129**, 507 (1998).
 - ² J. Shen, Z. Gaib, and J. Kirschner, *Surf. Sci. Rep.* **52**, 163 (2004).
 - ³ P. Ohresser, J. Shen, J. Barthel, M. Zheng, C. Mohan, M. Klaua, and J. Kirschner, *Phys. Rev. B* **59**, 3696 (1999).
 - ⁴ R. K. Singh and J. Narayan, *Phys. Rev. B* **41**, 8843 (1990).
 - ⁵ H. L. Meyerheim, M. Przybylski, A. Ernst, Y. Shi, J. Henk, E. Soyka, and J. Kirschner, *Phys. Rev. B* **76**, 035425 (2007).
 - ⁶ C. Chappert, D. Renard, P. Beauvillain, J. P. Renard, and J. Seiden, *J. Magn. Magn. Mater.* **54-57**, 795 (1986).
 - ⁷ L. Cagnon, T. Devolder, R. Cortes, A. Morrone, J. E. Schmidt, C. Chappert, and P. Allongue, *Phys. Rev. B* **63**, 104419 (2001).
 - ⁸ O. Fruchart, M. Eleoui, P.-O. Jubert, P. David, V. Santonacci, F. Cheynis, B. Borca, M. Hasegawa, and C. Meyer, *J. Phys.: Condens. Matter* **19**, 053001 (2007).
 - ⁹ J. T. Cheung and H. Sankur, *CRC Critical Reviews in Solid State and Material Sciences* **15**, 63 (1988).
 - ¹⁰ C. Clavero, Ph.D. thesis, Universidad Autónoma de Madrid, Madrid, Spain (2007).
 - ¹¹ O. Fruchart, S. Jaren, and J. Rothman, *Appl. Surf. Sci.* **135**, 218 (1998).
 - ¹² J. C. Heyraud and J. J. Métois, *Surface Science* **100**, 519 (1980).
 - ¹³ A. R. Sandy, S. G. J. Mochrie, D. M. Zehner, K. G. Huang, and D. Gibbs, *Phys. Rev. B* **43**, 4667 (1991).
 - ¹⁴ J. V. Barth, H. Brune, G. Ertl, and R. J. Behm, *Phys. Rev. B* **42**, 9307 (1990).
 - ¹⁵ F. Nouvertné, U. May, M. Bamming, A. Rampe, U. Korte, G. Guntherodt, R. Pentcheva, and M. Scheffler (1999).
 - ¹⁶ R. Vardavas, C. Ratsch, and R. Caflisch, *Surface Science* **569**, 185 (2004), ISSN 0039-6028.
 - ¹⁷ B. Voigtländer, G. Meyer, and N. M. Amer, *Phys. Rev. B* **44**, 10354 (1991).
 - ¹⁸ V. Repain, G. Baudot, H. Ellmer, and S. Rousset, *Mater. Sci. Engrg. B* **96**, 178 (2002).
 - ¹⁹ O. Fruchart, G. Renaud, J.-P. Deville, A. Barbier, F. Scheurer, M. Klaua, J. Barthel, M. Noblet, O. Ulrich, J. Mane-Mane, and J. Kirschner, *J. Cryst. Growth* **237-239**, 2035 (2002).
 - ²⁰ P. O. Jubert, O. Fruchart, and C. Meyer, *Surface Science* **522**, 8 (2003).
 - ²¹ O. Fruchart, G. Renaud, A. Barbier, M. Noblet, O. Ulrich, J.-P. Deville, F. Scheurer, J. Mane-Mane, V. Repain, G. Baudot, and S. Rousset, *Europhys. Lett.* **63**, 275 (2003).
 - ²² C. Cesari, J. P. Faure, G. Nihoul, K. Le Dang, P. Veillet, and D. Renard, *J. Magn. Magn. Mater.* **78**, 296 (1989).
 - ²³ S. Padovani, I. Chado, F. Scheurer, and J.-P. Bucher, *Phys. Rev. B* **59**, 11887 (1999).
 - ²⁴ U. Gradmann and J. Müller, *Phys. Stat. Sol.* **27**, 313 (1968).
 - ²⁵ U. Gradmann, in *Handbook of magnetic materials*, edited by K. H. J. Buschow (Elsevier Science Publishers B. V., North Holland, 1993), vol. 7, chap. 1, pp. 1-96.
 - ²⁶ D. Givord, M. Rossignol, and V. M. T. S. Barthem, *J. Magn. Magn. Mater.* **258-259**, 1 (2003).
 - ²⁷ J. Ferré, V. Grolier, P. Meyer, S. Lemerle, A. Maziewski, E. Stefanowicz, S. V. Tarasenko, V. V. Tarasenko, M. Kisielewski, and D. Renard, *Phys. Rev. B* **55**, 15092 (1997).
 - ²⁸ P. Bruno, G. Bayreuther, P. Beauvillain, C. Chappert, G. Lugert, D. Renard, J. P. Renard, and J. Seiden, *J. Appl. Phys.* **68**, 5759 (1990).
 - ²⁹ G. Bayreuther, P. Bruno, G. Lugert, and C. Turtur, *Phys. Rev. B* **40**, 7399 (1989).
 - ³⁰ J. Ferré, G. Pénissard, C. Marlière, D. Renard, P. Beauvillain, and J. P. Renard, *Appl. Phys. Lett.* **56**, 1588 (1990).
 - ³¹ Š. Višňovský, M. Nývlt, V. Prosser, R. Atkinson, W. R. Hendren, I. W. Salter, and M. J. Walker, *J. Appl. Phys.* **75**, 6783 (1994).
 - ³² Š. Višňovský, M. Nývlt, V. Prosser, J. Ferré, G. Pénissard, D. Renard, and G. Sczigel, *J. Magn. Mag. Mat.* **128**, 179 (1993).
 - ³³ Š. Višňovský, M. Nývlt, V. Prosser, R. Lopušník, R. Urban, J. Ferré, G. Pénissard, D. Renard, and R. Krishnan, *Phys. Rev. B* **52**, 1090 (1995).
 - ³⁴ J. Hamrle, M. Nývlt, Š. Višňovský, R. Urban, P. Beauvillain, R. Mégy, J. Ferré, L. Polerecký, and D. Renard, *Phys. Rev. B* **64**, 155405 (2001).
 - ³⁵ H. Takeshita, Y. Suzuki, H. Akinaga, W. Mizutani, K. Tanaka, T. Katayama, and A. Itoh, *Appl. Phys. Lett.* **68**, 3040 (1996).
 - ³⁶ C. Clavero, L. Martínez, A. García-Martín, J. M. García-Martín, Y. Huttel, N. D. Telling, G. van der Laan, A. Ce-bollada, and G. Armelles, *Phys. Rev. B* **77**, 094417 (2008).
 - ³⁷ M. Schubert, *Phys. Rev. B* **53**, 4265 (1996).
 - ³⁸ R. F. C. F. A. C. D. Weller, G. R. Harp and J. Sticht, *Phys. Rev. Lett.* **72**, 2097 (1994).
 - ³⁹ J. H. Weaver, C. Krafka, D. W. Lynch, and E. E. Koch, *Physics Daten* **18-1** (1981).